UPDATES TO THE PREDICTIVE MATERIAL MODELING SOFTWARE TOOLS

Arnaud Borner, Jeremie B. E. Meurisse, Georgios Bellas-Chatzigeorgis, Bruno Dias, Sergio Fraile Izquierdo, Federico Semeraro, Krishnan Swaminathan Gopalan, John M. Thornton, Nagi N. Mansour

Analytical Mechanics Associates, Inc.,
Thermal Protection Materials Branch,
NASA Ames Research Center

ABSTRACT

Updates on NASA's efforts to build predictive material models from the micro-scale to the macro-scale are presented. To complement the mission design cycle process and reduce the need for extensive testing, NASA is developing modeling and simulation tools that enable characterizing material properties and response to hot plasma experienced during atmospheric entry. The PuMA (microstructure analysis), PATO (macroscale material response), SPARTA (direct simulation Monte Carlo) and ARCHeS (arc heater modeling) codes are described. A range of applications, encompassing calculating effective material properties, study of high shear boundary layer flow over woven materials, new model of silicone-based coatings, new model of mechanical erosion, as well as approach to loose multi-physics coupling, are presented.

Index Terms— PuMA, PATO, SPARTA, ARCHeS

1. INTRODUCTION

The Predictive Material Modeling (PMM) effort is part of the Entry Systems Modeling (ESM) project under NASA's Game Changing Development (GCD) program. A suite of computing tools has been either created or co-developed under the PMM framework. These tools include microscale analysis (PuMA), macroscale material response analysis (PATO), direct simulation Monte Carlo (SPARTA), as well as arc heater modeling (ARCHeS). Moreover, various coupling pathways have been implemented in a common framework to automate linking between the PMM tools, as well as other NASA software. This paper will detail the various tools, as well as their use in some recent NASA applications.

2. SOFTWARE TOOLS

2.1. PuMA

The Porous Microstructure Analysis (PuMA) open-source software was developed to provide a robust and efficient framework for computing material properties based on 3D microstructures. The development was motivated by advancements in X-ray microtomography, an imaging technology that can resolve the structure of a material at a submicron scale, in 3D, and even in 4D (over time). Over the past decade, this technique has revolutionized the field of materials science for its ability to non-destructively analyze a material microstructure as well as provide digitized data on the geometry of the microstructure. It has provided insights into materials relevant to several NASA missions, including heatshields, parachute fabrics, meteorites, and other advanced composites, such as shown in Figure 1.

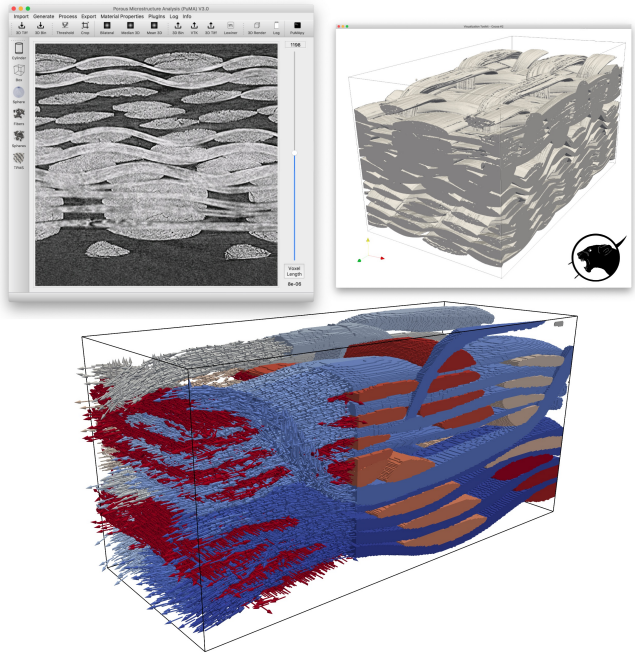

Fig. 1. Micro-CT woven Thermal Protection System (TPS) imported in the PuMA GUI, 3D rendered using thresholding, and post-processed with two segmentation and orientation detection [1].

PuMA, in its current version 3 [2], provides the capability of computing a comprehensive spectrum of properties, from the most fundamental geometric features of a microstructure to advanced anisotropic thermo-elastic and chemical behavior. Specifically, the software can compute morphological properties (e.g. specific surface area, volume fractions, mean intercept length, orientation), and physical properties (e.g. conductivity, elasticity, permeability, tortuosity), as well as simulate the material decomposition (e.g. oxidation, surface chemistry). The software can generate artificial microstructures, ranging from simple analytical shapes to complex fibrous woven and non-woven geometries. Coupling material generation and characterization enable parametric studies and sensitivity analysis to optimize the microstructural performance and inform design decisions and reliability assessment based on uncertainty quantification.

2.2. PATO

The Porous-material Analysis Toolbox based on OpenFOAM (PATO) software, an open-source research toolbox managed by the PMM team at NASA Ames Research Center, includes high-fidelity mass and heat transfer models for porous reactive materials containing several solid phases and a single gas phase [3]. Detailed chemical interactions occurring between the solid phases and the gas phase (i.e. solid pyrolysis, pyrolysis species injection in the gas phase, heterogeneous reactions between the solid phases and the gas phase, and homogeneous reactions in the gas phase) are modeled at the pore scale assuming Local Thermal Equilibrium (LTE). Chemistry is integrated in a macroscopic model derived by volume-averaging the governing equations for the conservation of solid mass, gas mass, momentum, energy, and either species when finite-rate chemistry is used or elements when equilibrium chemistry is used. PATO exists as a module of the open-source Computational Fluid Dynamics (CFD) software OpenFOAM. It dynamically links to the open-source library Mutation++, produced by the von Karman Institute for Fluid Dynamics, to compute equilibrium chemistry compositions along with thermodynamic and transport properties [4]. PATO is capable of using finite-rate chemistry to model gas surface interactions, but equilibrium chemistry is more commonly used [5]. It has been verified against the Fully Implicit Ablation and Thermal Analysis (FIAT) software, NASA's state-of-the-art code for TPS response modeling, which has been extensively validated based on arc-jet tests and flight data [6]. Three main strategies have addressed the flow/material coupling problem: 1) decoupled, standalone solvers for material and flow domains, 2) weak or strong coupling between standalone solvers, and 3) unified solvers. The first, and most popular strategy, consists of decoupling the flow field entirely from the material response and solving each domain utilizing CFD solvers for the environment and ablator thermal response solvers for the material. The second strategy consists of loosely coupling the flow and material response [7, 8, 9, 10], assuming that the flow field adapts instantaneously to material shape change. The third and more complex strategy relies on generalizing the governing equations to solve the flow field and the material in a unified approach [11, 12, 13]. Due to the strong coupling between each phase, this approach mitigates several Gas-Surface Interaction (GSI) assumptions from the previous strategies, making it possible to distinguish the competition between volume and surface ablation, which is impossible with the former two methods. The unified solver, currently under development in PATO, has been verified for simple test cases, including a porous plug geometry and the Beavers and Joseph problem [14]. Results were compared to Ref. [15], and show good agreement. More details about the unified solver, particularly the governing equations using the Volume Average Navier-Stokes equations, will be published in the near future.

2.3. SPARTA

SPARTA is an open-source direct simulation Monte Carlo (DSMC) code managed by Sandia National Laboratories with contributions from NASA Ames [16]. It is largely an efficient implementation of Bird's 1994 formulation [17], with the initial goal of running DSMC efficiently on the largest available supercomputers. Recently, this has included the development of DSMC kernels that can run on GPUs and multi-core CPUs via Cuda and OpenMP threading. SPARTA has been used to run the largest DSMC simulations that have been reported [16], with up to one hundred billion particles and billions of grid cells. SPARTA also supports models with billions of surface elements. A secondary goal was to make it easy to add new capabilities to SPARTA, so that the code can be used as an open research platform for users and developers to implement and test new models. These include, amongst others, different gas/surface collision/chemistry models or boundary conditions. SPARTA uses a multi-level hierarchical rectilinear grid with cut/split embedding of surface elements (triangles in 3D, line segments in 2D, or 2D axisymmetric). It also implements two kinds of surface elements: explicit, which is the standard definition of surface elements from a CAD-like input file, or implicit, defined by level-set values on grid corner points, which can be input from a voxelated image of a physical object. A Marching Cubes algorithm is used to create triangles in each grid cell. SPARTA is also used for computations of high altitude / low density rarefied hypersonic flows. It has been used to compute early trajectory times for both Mars Science Laboratory (MSL) and Mars 2020 missions (see Fig. 2), as well as other space missions, and mission concept investigations, in particular for Venus [18].

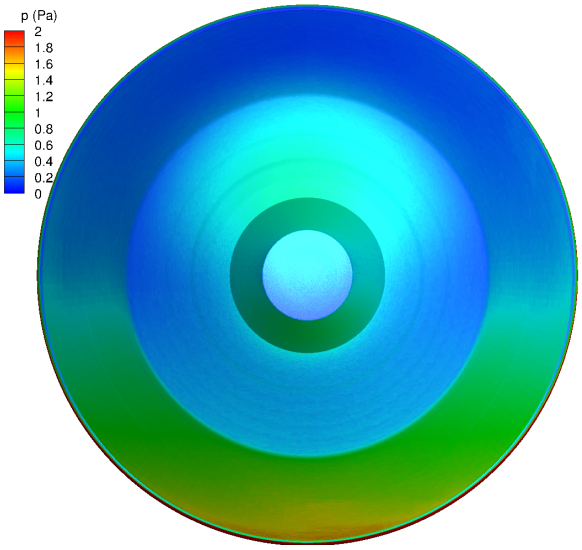

Fig. 2. Pressure on the backshell of Mars 2020 at t=39 s post Entry Interface, computed from SPARTA.

2.4. ARCHeS

The ARC Heater Simulator (ARCHeS) analysis tool provides a parallel, unstructured, finite volume solver based on the OpenFOAM library. ARCHeS includes the solution of line-by-line, or tabulated binned, three-dimensional radiative transfer, imposed current density, imposed magnetic field, external magnetic field, and turbulence models. Once again, Mutation++ is used to compute the equilibrium gas mixture composition as well as thermodynamic and transport properties. Three-dimensional and time-dependent simulations presented in this work show plasma instabilities in the constrictor of the arc heater. Analysis of the electric arc dynamics will provide a better intuitive understanding of the complex behavior of plasma flow observed in arc jets. Massively parallel and efficient simulation capability in ARCHeS allows long-time integration, necessary for the development of the plasma instabilities. The formulation used in ARCHeS has been demonstrated to be efficient to attain convergence on very stiff non-linear systems encountered in plasma flow simulations [19]. The unsteady flow is simulated from the anode chamber to the nozzle throat. LTE is assumed in the high-pressure arc heater. The imposed electric potential, the imposed magnetic field, and the external magnetic field are computed through Maxwell equations using a generalized geometric-algebraic multi-grid solver and are coupled to the flow through the Navier-Stokes equations. The three-dimensional radiation is solved using an accurate multi-band spectral discretization and Gaussian quadrature directional discretization. The inlet mass flux and the total current were chosen to be close to the operating conditions of large arc jet complexes used for TPS performance evaluation. One of the major conclusions from a recently published manuscript [19] is that capturing the arc instabilities enables describing the arc behavior and attachment at the cathodes without the need of a reattachment model. The magnetic field plays an essential role in the flow characterization from the anode chamber to the nozzle throat. The location and frequency of the arc attachment at the cathodes are mainly driven by upstream arc instabilities.

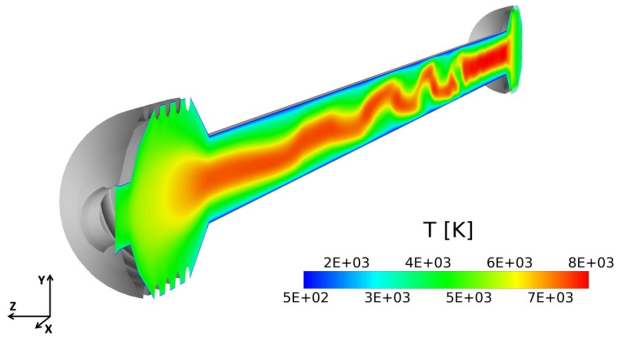

Fig. 3. Cutting plane of the temperature inside an arc jet heater, from the anode chamber to the nozzle throat [19].

3. APPLICATIONS

This section will offer a glimpse of the various applications that currently use the PMM software tools at NASA Ames Research Center.

3.1. Effective material properties with PuMA

The characterization of TPS materials is a fundamental, and often onerous, step in the design of new heatshields. PuMA offers a comprehensive suite of functionalities that enable computing homogenized material properties starting from a digital 3D geometry of the material microstructure. As previously mentioned, this voxel representation can either come directly from micro-CT, or it can be artificially generated using the synthetic generator functions that are part of PuMA or can be added to PuMA.

Figure 4 shows three important properties that are relevant to NASA heatshield applications, namely effective thermal conductivity, elasticity, and permeability. These physical properties are governed by Laplace's equation for steady-state heat conduction, Newton's equation for linear static elasticity, and Stokes' equation for slow creeping flow. The computation of the first two is based on similar finite volume numerical methods, respectively called the Multi-Point Flux Approximation (MPFA) and Multi-Point Stress Approximation (MPSA), whereas the third one relies on a Q1-Q1 finite element method. At a high level, the homogenization process is carried out in a similar way for all these properties, by enforcing a gradient across a Representative Elementary

Volume (REV) with periodic boundary conditions, converging the solution to steady state, and then averaging the corresponding quantity (i.e. converged flux, stress, or velocity) throughout the microstructure. Some examples of this procedure are shown in Figure 4: the effective conductivities of FiberForm (precursor of PICA [20]) and the ADEPT [21] weave were computed by running simulations across the three Cartesian axes; similarly, by imposing a displacement gradient, the mechanical properties of an artificial weave resembling a 3D Mid-Density Carbon Phenolic (3MDCP) TPS [22] were computed for the different phases and scales (phenolic resin, fiber-resin interaction, and woven unit cell); finally, the permeability of FiberForm was also computed, as shown by the pressure and velocity fields estimated by the software.

3.2. High Shear Boundary Layer Flow over woven TPS

There are many mechanisms by which the TPS material erodes – reaction with atmospheric gases, sublimation, and spallation. Spallation is a mechanism by which small chunks of material get removed due to the gas flow. This reduces the ability of the TPS material to protect the spacecraft as well as causes turbulence in the flow causing higher heating rates. In this application, we compute heat flux, pressure, and shear stress on the surface of weave fibers immersed in boundary layer flow over ablated TPS material, as a part of an over-arching goal to develop a spallation model for woven TPS material.

The TPS microstructure geometries were obtained at various stages of erosion using PuMA oxidation module and are imported into SPARTA. The flow over the fibers uses a boundary layer profile obtained from a CFD simulation of Earth entry conditions over the Mars Sample Return (MSR) Earth Entry Vehicle (EEV) spacecraft. This profile is provided as an input condition to the DSMC at the inlet and outlet boundaries. The gas is assumed to be fully dissociated and the surface temperature is assumed to be 3250 K. A fully diffuse scattering boundary condition is applied on the surface of the fibers. At steady state, there are around 13 million particles in the domain. Once steady state is reached, the final data is averaged over 100,000 time steps to obtain good averages.

Fig. 5 shows the DSMC simulation results of heat flux during boundary layer flow over chemically eroded woven TPS material with and without resin. The heat flux for the case with the resin is about 50% higher than the case without the resin. Similar plots showing the shear stress are presented in Fig. 6. We find that the shear stresses are higher in the case of TPS with resin by a factor of about four. It is also interesting to note that the maximum heat flux is located at the leading edge, while the maximum shear stresses occur at the trailing edge. The ability of the flow to penetrate into the microstructure in the case where there is no resin allows for a much higher dissipation area leading to lower shear stresses and heat flux loads. Thus, the TPS material with the resin is more susceptible to mass loss due to spallation.

3.3. PICA-NuSil modeling

The heatshields of the MSL and Mars 2020 missions were made out of Phenolic Impregnated Carbon Ablator (PICA), a lightweight ablator developed at the NASA Ames Research Center to protect entry capsules from the severe environment encountered during atmospheric entry. Both heatshields and instrumentation plugs of these missions were lightly sprayed with NuSil CV-1144-0 (NuSil), a space-grade silicone-based coating. The primary purpose of the thin coating is to act as a sealant for dust suppression during clean room operations. Despite its less than a millimeter thickness, NuSil alters the thermal response of the TPS, generating the need for the development of a new PICA-NuSil model (PICA-N) essential for the accurate interpretation of experimental data and TPS sizing of future missions.

To support the development of the PICA-N model, dedicated arc jet experimental campaigns have been conducted, with the first one being at NASA's Langley Hypersonic Materials Environmental Test System (HyMETS) arc jet facility, generating critical data for characterizing the thermal response of coated PICA [25]. In the original uncoated PICA simulations, thermochemical ablation was calculated using B' quantities assuming purely carbon graphite charred surface. Based on phenomenological observations and the fact that silicon oxycarbide layers transform mainly into domains of SiO_2 due to their interaction with the boundary layer species, charred NuSil was modeled as a SiO_2 interface till its complete removal, requiring the original single component formulation of the Mutation++ surface mass balance solver to be extended to multi-component surfaces [26, 27]. The thickness of the coating affects only the surface response and not the bulk PICA, which was modeled based on the extensively validated work of Milos *et al.* [28], used in all missions with PICA as heatshield.

One of the twelve experimental cases of the HyMETS campaign that was used to develop the PICA-N model for air is shown in Fig. 7. The experimental conditions were 140 W/cm^2 cold-wall heat flux and pressure of 5600 Pa with air as the testing gas. The boundary conditions for the material response were obtained from CFD simulations, giving pressure, non-dimensional heat transfer coefficient, and boundary layer edge enthalpy around the test sample. It was observed that during the first 20 seconds, the NuSil coating remained on the sample providing extra protection. After its first removal at the stagnation line, the surface temperature and recession increased. At the end of the heating process (30 seconds), the coating was only removed in a disk around the stagnation line. PATO simulations showed good agreement with experimental results, predicting two temperature plateaus, the temperature jump location, and the total recession of 1.93 mm.

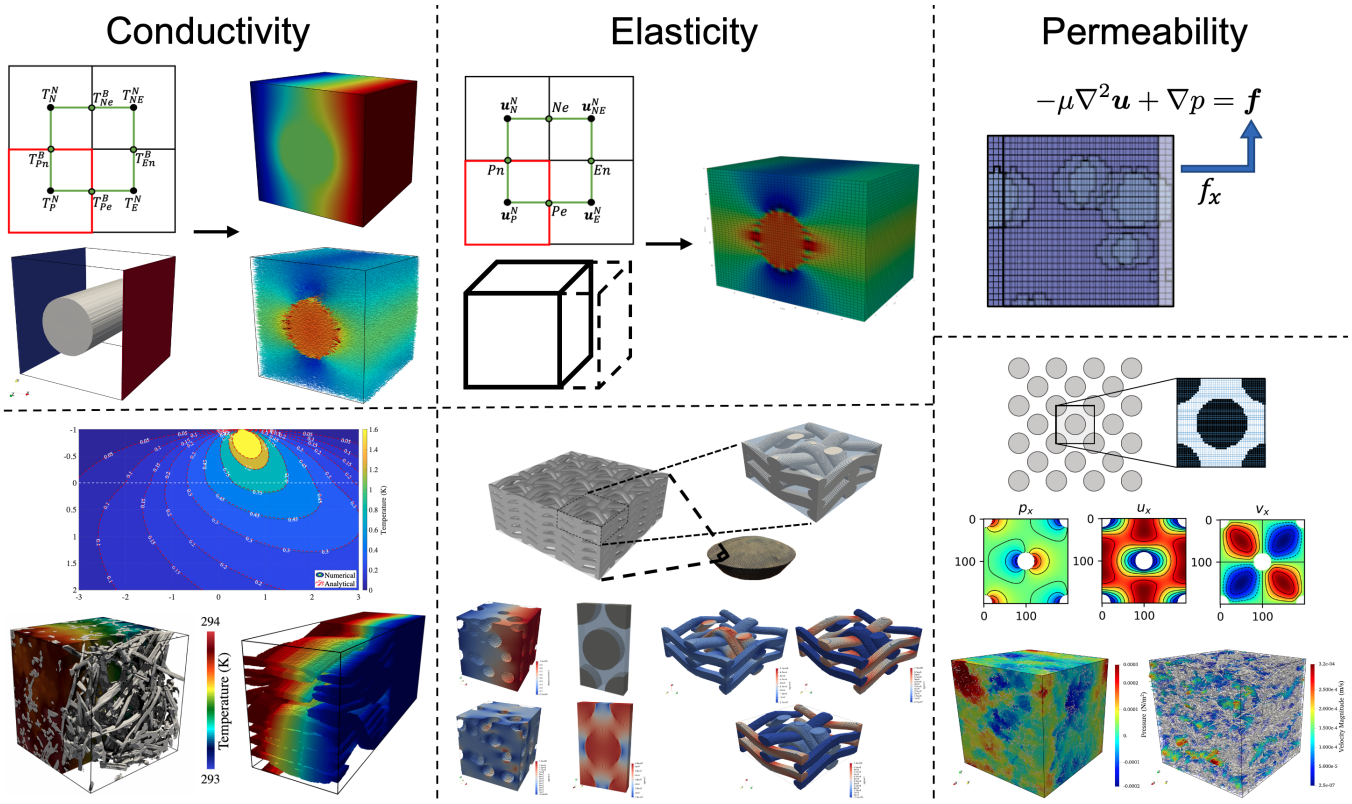

Fig. 4. Some advanced material properties that PuMA can compute: conductivity [23], elasticity [24], and permeability. The top row shows the methods used for homogenization, while the bottom row shows the Verification and Validation (V&V) exercises that were performed on some 3D geometries relevant to NASA.

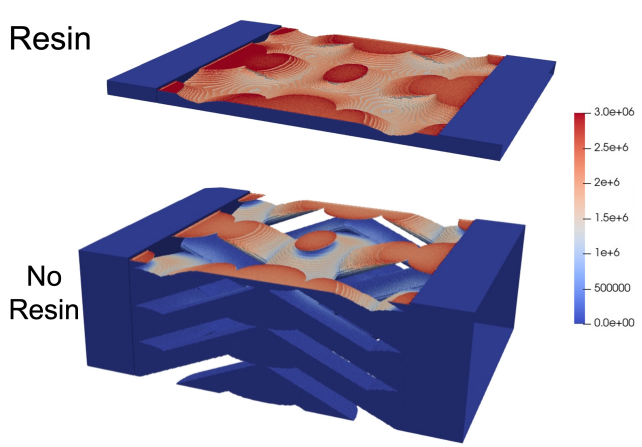

Fig. 5. DSMC results of heat flux during boundary layer flow over chemically eroded woven TPS material with and without resin.

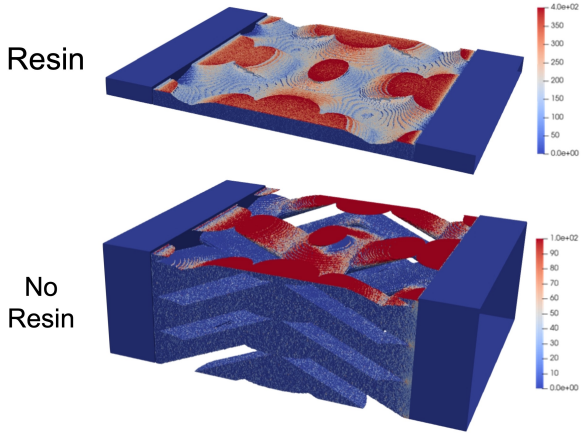

Fig. 6. DSMC results of shear stress during boundary layer flow over chemically eroded woven TPS material with and without resin.

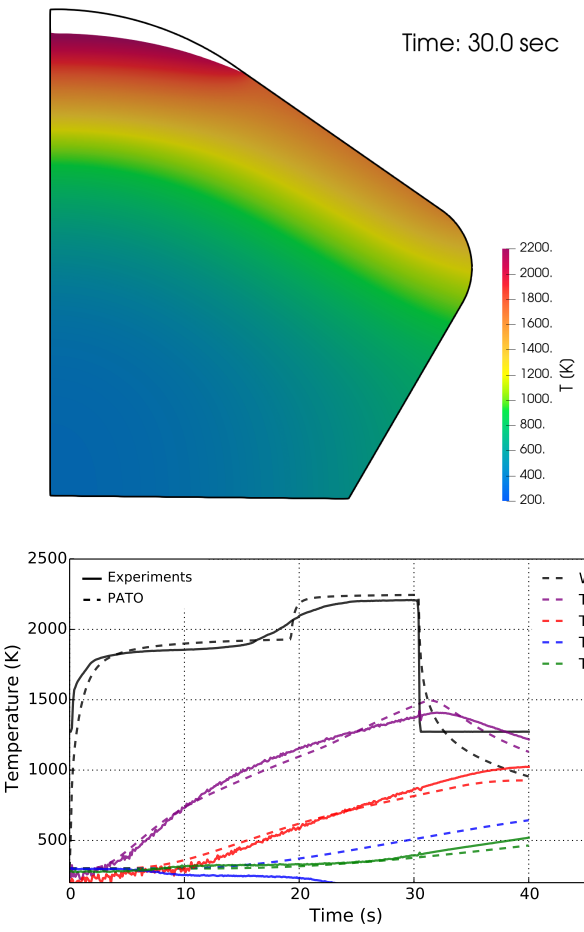

Fig. 7. Simulation of HyMETS conditions using the PICA-N model in air, showing temperature field and stagnation line profile compared to experimental results.

An accurate PICA-N model will be paramount for the correct interpretation of the Mars Entry, Descent, and Landing Instrumentation 1 and 2 (MEDLI and MEDLI2) in-flight data of the MSL and Mars2020 missions. These in-flight data are important for the validation of state-of-the-art aerothermodynamics models and sizing of future NASA missions.

3.4. Mechanical erosion modeling

For ablative thermal protection materials, the term mechanical erosion, also known as spallation, refers to the physical ejection of solid particles from the ablating surface. This results in an increased total surface recession and must be taken into account for heatshield modeling under high-shear conditions. This phenomenon has been extensively studied in the literature over the last decades by numerous authors [29, 30, 31, 32, 33]. Three mechanisms have been identified as the main cause: the shear stress induced by the flow, the normal stress induced by pyrolysis gas build-up, and the thermal stress induced by the material's temperature field. The mechanical erosion model implemented in PATO accounts for the potential mass removal due to high-shear entry conditions at the macro-scale. The modeling process can be broken down into the steps described in the following paragraphs.

The mechanical properties of the material are loaded into the model as a function of the temperature field already computed by PATO. In the case of orthotropic materials, their orientation is also obtained for each cell to account for different TPS material laying processes.

The implemented stress analysis solver computes stresses and displacement fields within the material using CFD-provided wall shear stress and pressure values as surface boundary conditions. This solver is suitable for linear isotropic and orthotropic materials and was verified against analytical results found in the literature.

The resultant stresses may lead to material failure and mechanical erosion, particularly near the surface of TPS materials, where the oxidized fibers have thinned and are mechanically weaker. The relative importance of mechanical erosion compared to the rest of the ablation processes is still unknown in the literature. Recent experimental campaigns and numerical simulations [34, 35] are attempting to answer this question. The developed model identifies failed regions on the surface with stresses, computed using the stress analysis solver coupled to the material response, that exceed the material's ultimate strength. This failure criteria model was chosen as a first approach for determining spalling regions. Mechanical erosion is caused by brittle failure of the fibers, for which maximum stress theories work well, but the uncertainties related to the maximum stress model still need to be evaluated for this application.

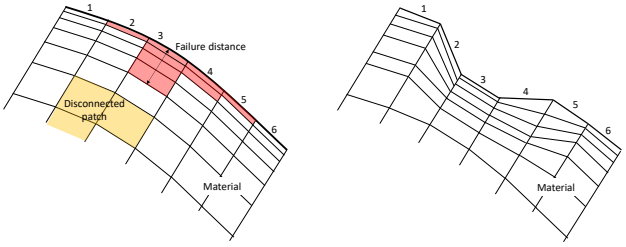

(a) Undeformed failing material. (b) Deformed material.

Fig. 8. Schematic for material failure.

The failure criteria model gives each computational cell information on whether it is failing. Furthermore, this data is used by the mass removal model to deform the mesh thus removing the failed material, as can be observed in Fig. 8. The coupling of all solvers enables the simulation of the total recession of TPS materials due to surface chemistry and mechanical erosion.

3.5. Loosely coupled environment and material response

During atmospheric entry, interactions occur between the aerothermal environment and material response. However, due to computational limitations, these are generally decoupled and computed separately with a blowing correction term introduced into the material response model to account for the blowing of char and pyrolysis gases from the heatshield into the environment [36]. A loosely coupled approach is under development which has the potential to add increased fidelity in predictive material modeling by accounting for blowing gases at the heatshield surface. Insights into the blowing gases may also lead to a reduction in uncertainty when decoupling the environment and material response.

The coupled approach makes use of a blowing boundary condition in the Data Parallel Line Relaxation (DPLR) code, which is used in computing the aerothermal environment [37]. At each time point along the trajectory, the workflow is divided into the following steps which are illustrated in Fig. 9. First, environment properties are computed using DPLR. Second, radiative heating is computed via the Nonequilibrium Radiative Transport and Spectra (NEQAIR) program [38, 39, 40]. Third, the thermal response inside the material is computed using PATO with the computed environment properties, radiative heating, and a blowing correction. In the fourth step, the blowing gases computed by PATO at the heatshield surface are used as inputs for the blowing boundary condition in DPLR to compute new environment properties. Radiative heating is then recomputed with NEQAIR. Lastly, the updated environments are used to compute a new thermal response in PATO without blowing correction which provides new conditions for the blowing boundary in DPLR. The fourth, fifth, and sixth steps are then repeated until convergence in radiative heating and surface temperature is obtained.

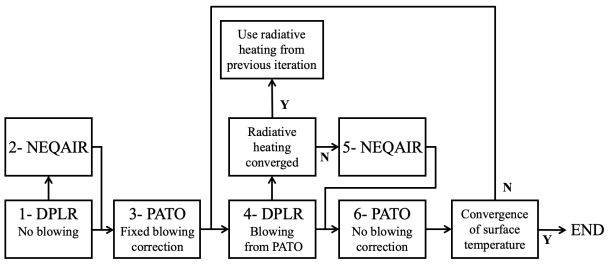

Fig. 9. Steps in coupling between CFD and material response.

The coupled approach has been used in computing the 3D material response for the MSL entry into the Martian atmosphere. The numerical simulations were obtained using NASA's Pleiades supercomputer. Differences in the surface temperature and pyrolysis gas blowing rate at 65s after the entry interface can be seen in Figs. 10 and 11 for the uncoupled and coupled approaches.

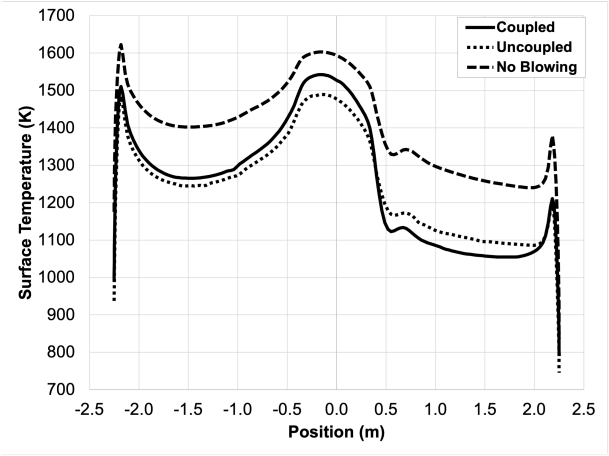

Fig. 10. Centerline plot of surface temperature 65s after the entry interface.

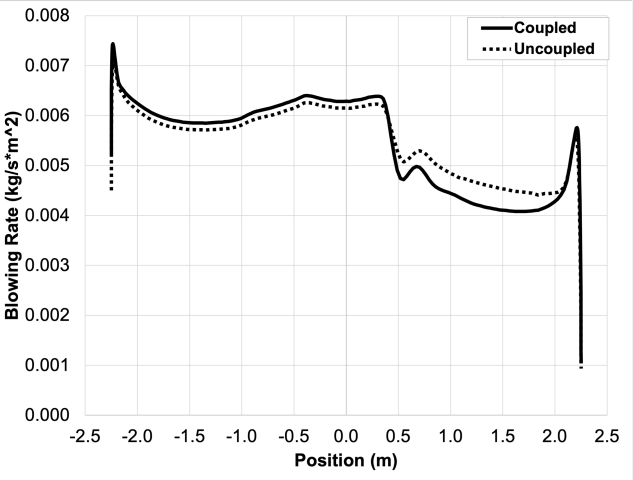

Fig. 11. Centerline plot of pyrolysis gas blowing 65s after the entry interface.

4. ACKNOWLEDGMENTS

This work was supported by the Entry System Modeling project (M.D. Barnhardt project manager, A. Brandis principal investigator) as part of the NASA Game Changing Development program. The authors were funded by NASA contract NNA15BB15C to Analytical Mechanics Associates (AMA), Inc.

5. REFERENCES

[1] F. Semeraro, J.C. Ferguson, F. Panerai, R.J. King, and N.N. Mansour, "Anisotropic analysis of fibrous and woven materials part 1: Estimation of local orientation," *Computational Materials Science*, vol. 178, pp. 109631, 2020.

[2] J.C. Ferguson, F. Semeraro, J.M. Thornton, F. Panerai, A. Borner, and N.N. Mansour, "Update 3.0 to "PuMA: The Porous Microstructure Analysis software"," *SoftwareX*, vol. 15, pp. 100775, 2021.

[3] J. Lachaud, J.B. Scoggins, T.E. Magin, M.G. Meyer, and N.N. Mansour, "A generic local thermal equilibrium model for porous reactive materials submitted to high temperatures," *International Journal of Heat and Mass Transfer*, vol. 108, pp. 1406–1417, may 2017.

[4] J.B. Scoggins, V. Leroy, G. Bellas-Chatzigeorgis, B. Dias, and T.E. Magin, "Mutation++: MUlticomponent Thermodynamic And Transport properties for IONized gases in C++," *arXiv:2002.01783v1 [physics.comp-ph]*, 2020.

[5] J. Lachaud, T. van Eekelen, J.B. Scoggins, T.E. Magin, and N.N. Mansour, "Detailed chemical equilibrium model for porous ablative materials," *International Journal of Heat and Mass Transfer*, vol. 90, pp. 1034–1045, nov 2015.

[6] A.D. Omidy, F. Panerai, Al. Martin, J. Lachaud, I. Cozmuta, and N.N. Mansour, "Code-to-code comparison, and material response modeling of Stardust and MSL using PATO and FIAT," Tech. Rep., No. NASA/CR-2015-218960, 2015.

[7] Y.-K. Chen and T. Gökçen, "Implicit Coupling Approach for Simulation of Charring Carbon Ablators," *Journal of Spacecraft and Rockets*, vol. 51, no. 3, pp. 779–788, may 2014.

[8] B. Dias, A. Turchi, E.C. Stern, and T.E. Magin, "A model for meteoroid ablation including melting and vaporization," *Icarus*, vol. 345, pp. 113710, jul 2020.

[9] P. Schrooyen, A. Turchi, K. Hillewaert, P. Chatelain, and T.E. Magin, "Two-way coupled simulations of stagnation-point ablation with transient material response," *International Journal of Thermal Sciences*, vol. 134, pp. 639 – 652, 2018.

[10] J.M. Thornton, J.B.E. Meurisse, D.K. Prabhu, A. Borner, J.D. Monk, N.N. Mansour, and B.A. Cruden, "Analysis of the MSL/MEDLI Entry Data with Coupled CFD and Material Response," *18th International Planetary Probe Workshop*, 2021.

[11] P. Schrooyen, K. Hillewaert, T.E. Magin, and P. Chatelain, "Fully implicit Discontinuous Galerkin solver to study surface and volume ablation competition in atmospheric entry flows," *International Journal of Heat and Mass Transfer*, vol. 103, no. Supplement C, pp. 108 – 124, 2016.

[12] H. Weng and A. Martin, "Development of a Universal Solver and Its Application to Ablation Problems," in *47th AIAA Thermophysics Conference*. jun 2017, American Institute of Aeronautics and Astronautics.

[13] U. Duzel and A. Martin, "Modeling High Velocity Flow Through Porous Media," in *AIAA Scitech 2020 Forum*. jan 2020, American Institute of Aeronautics and Astronautics.

[14] G.S. Beavers and D.D. Joseph, "Boundary conditions at a naturally permeable wall," *Journal of fluid mechanics*, vol. 30, no. 1, pp. 197–207, 1967.

[15] L. Betchen, A. Straatman, and B. Thompson, "A Nonequilibrium Finite-Volume Model for Conjugate Fluid/Porous/Solid Domains," *Numerical Heat Transfer: Part A: Applications*, vol. 49, no. 6, pp. 543–565, sep 2006.

[16] S.J. Plimpton, S.G. Moore, A. Borner, A.K. Stagg, T.P. Koehler, J.R. Torczynski, and M.A. Gallis, "Direct simulation Monte Carlo on petaflop supercomputers and beyond," *Physics of Fluids*, vol. 31, no. 8, pp. 086101, 2019.

[17] G.A. Bird, *Molecular gas dynamics and the direct simulation of gas flows*, Clarendon Press, 1994.

[18] J. Rabinovitch, A. Borner, M.A. Gallis, and C. Sotin, "Hypervelocity Noble Gas Sampling in the Upper Atmosphere of Venus," in *AIAA Aviation 2019 Forum*, 2019, p. 3223.

[19] J.B.E. Meurisse, A.A. Laguna, M. Panesi, and N.N. Mansour, "Three-dimensional unsteady model of arc heater plasma flow," *Aerospace Science and Technology*, vol. 123, pp. 107465, 2022.

[20] H. Tran, C. Johnson, D. Rasky, F. Hui, and Y.-K. Hsu, M.-T.and Chen, "Phenolic impregnated carbon ablators (PICA) for Discovery Class missions," in *31st Thermophysics Conference*, 1996, p. 1911.

[21] E. Venkatapathy, K. Hamm, I. Fernandez, J. Arnold, D. Kinney, B.d Laub, A. Makino, M. McGuire, K. Peterson, D. Prabhu, et al., "Adaptive deployable entry and placement technology (ADEPT): a feasibility study for human missions to Mars," in *21st AIAA Aerodynamic Decelerator Systems Technology Conference and Seminar*, 2011, p. 2608.

[22] D. Ellerby, H. Hwang, M. Gasch, R. Beck, and T. White, "TPS and Entry Technologies for Future Outer Planet Exploration," *Planetary Science Decadal Community White Papers*, 2020.

[23] F. Semeraro, J.C. Ferguson, M. Acin, F. Panerai, and N.N. Mansour, "Anisotropic analysis of fibrous and woven materials part 2: Computation of effective conductivity," *Computational Materials Science*, vol. 186, pp. 109956, 2021.

[24] S. Fraile Izquierdo, F. Semeraro, and M. Acín, "Multi-Scale Analysis of Effective Mechanical Properties of Porous 3D Woven Composite Materials," in *AIAA SCITECH 2022 Forum*, 2022, p. 2281.

[25] B.K. Bessire, A. Borner, J.B. Meurisse, and J.D. Monk, "Progress Towards Modeling the Mars Science Laboratory PICA-NuSil Heatshield," *International Planetary Probe Workshop*, 2019.

[26] J.B.E. Meurisse, B. Bessire, J.D. Monk, F. Panerai, and N.N. Mansour, "Progress towards modeling the ablation response of NuSil-coated PICA," *Ablation Workshop, ARC-E-DAA-TN73344*, 2019.

[27] P.A. Ventura Diaz, J.B.E. Meurisse, A.M. Brandis, B.K. Bessire, M. Barnhardt, and S.Yoon, "High-Fidelity Simulations of HyMETS Arc-Jet Flows for PICA-N Modeling," in *AIAA Scitech 2021 Forum*, 2021, pp. 1–20.

[28] F.S. Milos and Y.-K. Chen, "Ablation and Thermal Response Property Model Validation for Phenolic Impregnated Carbon Ablator," *Journal of Spacecraft and Rockets*, vol. 47, no. 5, pp. 786–805, 2010.

[29] S.M. Scala and L.M. Gilbert, "Thermal degradation of a char-forming plastic during hypersonic flight," *ARS Journal*, vol. 32, no. 6, pp. 917–924, 1962.

[30] R.D. Mathieu, "Mechanical spallation of charring ablators in hyperthermal environments," *AIAA journal*, vol. 2, no. 9, pp. 1621–1627, 1964.

[31] P.J. Schneider, T.A. Dolton, and G.W. Reed, "Mechanical erosion of charring ablators in ground-test and re-entry environments," *AIAA Journal*, vol. 6, no. 1, pp. 64–72, 1968.

[32] J. Sullivan and W. Kobayashi, "Spallation modeling in the Charring Material Thermal Response and Ablation (CMA) computer program," in *22nd Thermophysics Conference*, 1987, p. 1516.

[33] R. Fu, H. Weng, J.F. Wenk, and A. Martin, "Thermomechanical coupling for charring ablators," *Journal of Thermophysics and Heat Transfer*, vol. 32, no. 2, pp. 369–379, 2018.

[34] A. Martin, S.C.C. Bailey, F. Panerai, R.S.C. Davuluri, H. Zhang, A.R. Vazsonyi, Z.S. Lippay, N.N. Mansour, J.A. Inman, B.F. Bathel, et al., "Numerical and experimental analysis of spallation phenomena," *CEAS Space Journal*, vol. 8, no. 4, pp. 229–236, 2016.

[35] F. Grigat, S. Loehle, F. Zander, and S. Fasoulas, "Detection of Spallation Phenomena on Ablator Surfaces," in *AIAA Scitech 2020 Forum*, 2020, p. 1706.

[36] Y.-K. Chen and F.S. Milos, "Ablation and Thermal Response Program for Spacecraft Heatshield Analysis," *Journal of Spacecraft and Rockets*, vol. 36, no. 3, pp. 475–483, 2020/05/17 1999.

[37] M.J. Wright, T. White, and N. Mangini, "Data Parallel Line Relaxation (DPLR) Code User Manual: Acadia-Version 4.01. 1," Tech. Rep. TM–2009-215388, NASA, October 2009.

[38] C. Park, "Nonequilibrium air radiation (NEQAIR) program: User's manual," Tech. Rep. NASA-TM-86707, NASA, July 1985.

[39] A.M. Brandis and B.A. Cruden, "NEQAIRv14.0 Release Notes: Nonequilibrium and Equilibrium Radiative Transport Spectra Program," Tech. Rep., NASA, November 2014.

[40] B.A. Cruden and A.M. Brandis, "Updates to the NEQAIR radiation solver," in *6th International Workshop on Radiation of High Temperature Gases in Atmospheric Entry*, 2014.